

# 1 **Self-organized emergence of hyaline cartilage in hiPSC-derived** 2 **multi-tissue organoids**

## 3 **Author Information**

---

4 Mancı Li<sup>1,2</sup>, Juan E. Abrahante<sup>3</sup>, Amanda Vegoe<sup>4,5,6</sup>, Yi Wen Chai<sup>4,5,6</sup>, Beth Lindborg<sup>4,5,6</sup>, Ferenc Toth<sup>7</sup>,  
5 Peter A. Larsen<sup>1,2</sup>, Timothy D. O'Brien<sup>4,5,6,\*</sup>

6

## 7 **Affiliations**

8 <sup>1</sup>Department of Veterinary and Biomedical Sciences, University of Minnesota, St. Paul, MN 55108

9 <sup>2</sup>Minnesota Center for Prion Research and Outreach, College of Veterinary Medicine, St. Paul, University  
10 of Minnesota, MN 55108

11 <sup>3</sup>University of Minnesota Informatics Institute, University of Minnesota, Minneapolis, MN 55455

12 <sup>4</sup>Stem Cell Institute, University of Minnesota, Minneapolis, MN 55455

13 <sup>5</sup>Department of Veterinary Population Medicine, University of Minnesota, St. Paul, MN 55108

14 <sup>6</sup>Sarcio, Inc., Minneapolis, MN 55455

15 <sup>7</sup>Department of Veterinary Clinical Sciences, University of Minnesota, St. Paul, MN 55108

## 16 **Contributions**

17 M.L., F.T., and T.D.O. wrote the manuscript. T.D.O., B.L., A.V. and Y.W.C. designed the experiments.

18 B.L., A.V., and Y.W.C. performed in vitro experiments and T.D.O. performed histology analysis. J.E.A.,

19 M.L., and P.A.L. analyzed RNA sequencing data. M.L. conducted data exploration, statistical analysis,

20 and data visualization. F.T., P.A.L., and T.D.O. provided critical revision of the manuscript and all

21 authors read and approved the final version of the manuscript.

22 Corresponding author:

23 Manci Li, BSc, PhD student

24 Department of Veterinary and Biomedical Sciences, University of Minnesota

25 1971 Commonwealth Avenue, St. Paul, MN 55108

26 email: [li000021@umn.edu](mailto:li000021@umn.edu)

27 phone: 612-626-1694

28 fax: 612-625-5203

29 \*Co-senior author

## 30 **Abstract**

---

31 Despite holding great therapeutic potential, existing protocols for *in vitro* chondrogenesis and hyaline  
32 cartilage production from human induced pluripotent stem cells (hiPSC) are laborious and complex with  
33 unclear long-term consequences. Here, we developed a simple xeno- and feeder-free protocol for human  
34 hyaline cartilage production *in vitro* using hydrogel-cultured multi-tissue organoids (MTOs). We  
35 investigate gene regulatory networks during spontaneous hiPSC-MTO differentiation using RNA  
36 sequencing and bioinformatic analyses. We find the interplays between BMPs and neural FGF pathways  
37 are associated with the phenotype transition of MTOs. We recognize TGF-beta/BMP and Wnt signaling  
38 likely contribute to the long-term maintenance of MTO cartilage growth and further adoption of articular  
39 cartilage development. By comparing the MTO transcriptome with human lower limb chondrocytes, we  
40 observe that the expression of chondrocyte-specific genes in MTO shows a strong correlation with fetal  
41 lower limb chondrocytes. Collectively, our findings describe the self-organized emergence of hyaline  
42 cartilage in MTO, its associated molecular pathways, and its spontaneous adoption of articular cartilage  
43 development trajectory.

## 44 **Introduction**

---

45 Cartilage tears and osteochondral defects involving the articular cartilage are common injuries that may  
46 lead to disabling osteoarthritis and subsequent joint replacement. Injured articular cartilage has a limited  
47 capacity for self-regeneration, and currently, available treatment options for symptomatic cartilage lesions  
48 are limited. Surgical repair methods such as osteochondral auto/allograft transplantation and bone marrow  
49 stimulation via microfracture all have their limitations including the scarcity of suitable grafts or their  
50 inability to yield repair tissues composed of hyaline- vs. fibrocartilage. To address these shortcomings,  
51 increasing efforts have recently focused on implementing cell-based methods for the treatment of articular  
52 cartilage injuries. First and second-generation autologous chondrocyte implantation methods have been  
53 shown to yield good patient outcomes, but the morbidity and cost associated with the surgical harvest of  
54 autologous chondrocytes for *in vitro* expansion remain critical drawbacks<sup>1</sup>.

55 In order to eliminate the pitfalls associated with the surgical harvest of autologous chondrocytes, studies  
56 have lately concentrated on *in vitro* chondrogenesis and hyaline cartilage production from human stem  
57 cells<sup>2,3</sup>. Specifically, human induced pluripotent stem cells (hiPSC) have been shown to have the potential  
58 to differentiate into chondrocytes; however, clinical translation of hiPSC derived chondrocytes still faces  
59 several challenges. The common approach for generating hiPSC-derived chondrocytes has been a 2D-3D  
60 sequential culture where hiPSC-derived mesodermal cells are cultured in monolayer before 3D—such as  
61 pellet<sup>4-7</sup> and suspension<sup>8,9</sup>—cell culture. Implementing 3D culturing in the process has been shown to  
62 improve the quality of the cartilage generated<sup>10</sup>. Nevertheless, these existing step-wise protocols are labor-  
63 intensive and involve the use of fetal bovine serum (FBS) as well as manipulations of inductive and  
64 repressive signals for mesoderm specification in embryonic development<sup>6</sup>. Moreover, the long-term  
65 maintenance and consequences of chondrocytes in suspension and pellet cell cultures remain to be  
66 explored.

67 Organoids are 3D cultures that realize the self-organizing potential of stem cells<sup>11,12</sup>. Several  
68 transcriptome analyses have shown that organoids can recapitulate a variety of early developmental

69 processes in human organs, such as brain<sup>13–17</sup>, retina<sup>18</sup>, kidney<sup>19</sup>, intestinal epithelium<sup>20</sup>, and trophoblast<sup>21</sup>.  
70 As chondrogenic tissue formation occurs at the highest levels during fetal/younger stages of life<sup>22</sup>, 3D  
71 organoid systems have a unique advantage in achieving *in vitro* chondrogenesis and even associated  
72 organization of extracellular matrices. *De novo* hyaline cartilage from bovine organoids has been recently  
73 reported and showed higher similarity to native cartilage<sup>10</sup>. Human clinical translation of organoid-  
74 derived hyaline cartilage and chondrocytes requires xenobiotic-free and serum-free culturing  
75 protocols<sup>23,24</sup>. Elucidation of key mesoderm formation pathways associated with cartilage production in  
76 organoids is needed to facilitate future cartilage production through organoid engineering.

77 Here, we report the spontaneous appearance—without the addition of external chemicals beyond those  
78 included in E8 medium—of hyaline cartilage in hiPSC-derived multi-tissue organoids (MTOs) using a  
79 modification of our previously reported method that employed Cell-Mate3D hydrogels and formed  
80 predominantly brain tissue<sup>25</sup>. To gain a better understanding of the molecular pathways in MTOs during  
81 *in vitro* cartilage production, we conducted RNA-Seq at weeks 8, 11, and 15 following MTOs induction.  
82 By comparing with existing RNA-seq data obtained from human lower limb chondrocytes at different life  
83 stages<sup>6,26–28</sup>, we demonstrate that the relevant gene expression in 15-week MTOs is strongly correlated  
84 with human fetal lower limb tissues. In summary, this study describes the spontaneous emergence of  
85 human hyaline cartilage from hiPSC-derived MTOs cultured with a xeno- and feeder- protocol and its  
86 associated molecular pathways.

## 87 **Results**

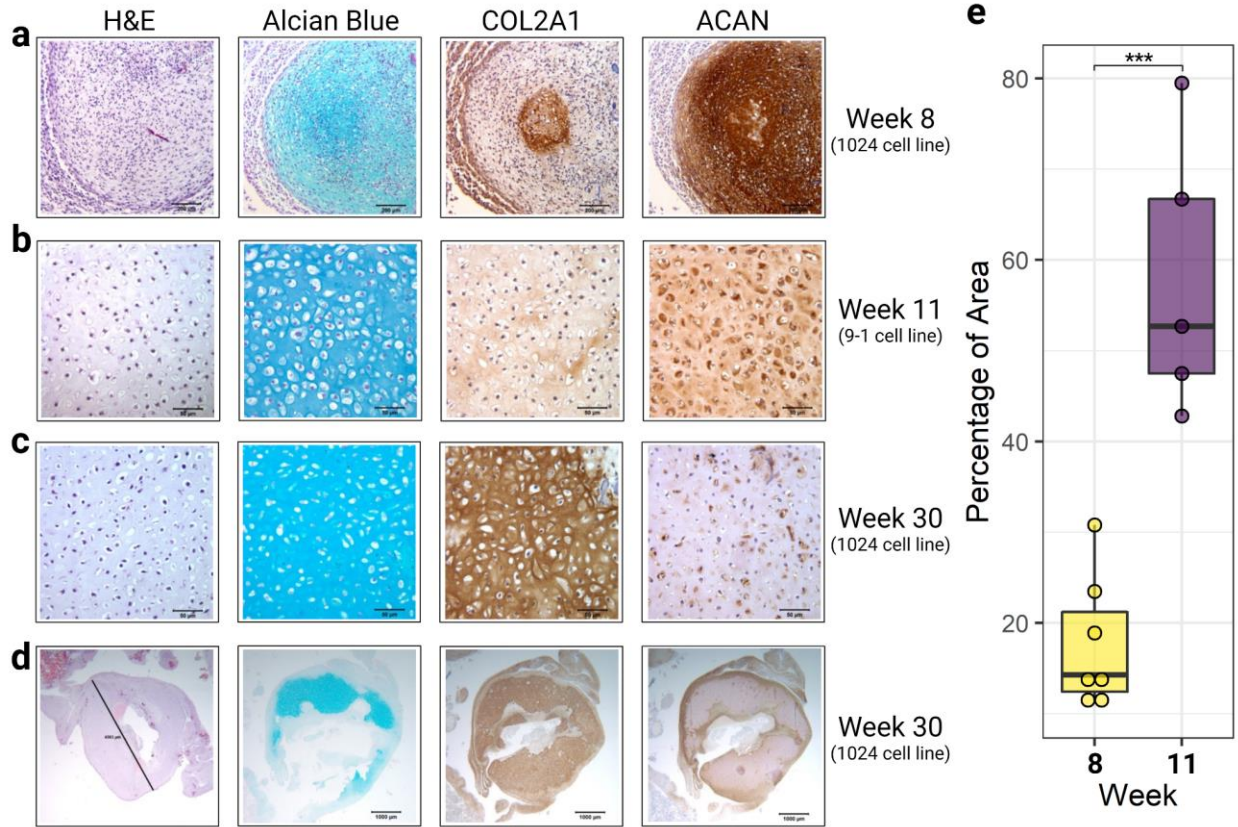
---

### 88 **Culturing hiPSC to cartilage producing MTO**

89 We have previously reported the generation of cerebral organoids (CO) from human pluripotent stem  
90 cells using a chemically defined hydrogel material (Cell-Mate3D) and culture medium (E8) and  
91 characterized their composition for up to 28 days from induction by which time they were approximately  
92 3mm in diameter<sup>25</sup>. However, the culture time span of these organoids was limited due to central necrosis  
93 of the organoids when they reached 2-3mm in diameter, presumably due to hypoxia. To address this  
94 limitation, we adapted our methods to use a bioreactor system that has a gas-permeable bottom  
95 (GREX100) thereby allowing oxygen diffusion from the bottom as well as the top of the culture medium  
96 interfaces. Using this system along with continued use of only E8 medium, we were able to routinely  
97 culture organoids for months, following some for up to 30 weeks (week 30). A further simplification of  
98 our originally reported method involved the elimination of the use of the chitosan component of the Cell-  
99 Mate3D  $\mu$ Gel. As early as week 6, we observed that, although the cerebral phenotype of the organoids  
100 was still prominent, cartilage-like tissues started to emerge—organoids with multiple tissue types are  
101 hereon referred to as multi-tissue organoids (MTOs) (Fig. S1). Notably, despite their apparent reduction  
102 in the relative proportion of total MTO tissue, neural tissues persisted in MTOs throughout the  
103 characterized period of development (Fig. S1). Cartilage, which formed centrally in the MTOs, was easily  
104 recognizable through histology due to its distinct morphology and characteristic histochemical and  
105 immunohistochemical features. The main types of cartilage—articular, hypertrophic, elastic, and fibrous  
106 cartilage—can be distinguished by the structure and composition of their extracellular matrix (ECM).  
107 Articular cartilage, for example, has a hyaline rather than fibrous morphology (fibrocartilage), and  
108 contains predominantly type II collagen, little or no type I collagen (fibrocartilage) or type X collagen  
109 (hypertrophic cartilage), and no elastic fibers. By week 8, hyaline cartilage became very distinguishable  
110 in MTOs, as indicated by the development of characteristic, abundant, homogenous pale basophilic  
111 extracellular matrix (ECM) in H&E stained sections (Fig. 1a) and prominent Alcian blue staining of

112 proteoglycan/hyaluronic acid components typical of cartilage ECM<sup>32</sup> (Fig. 1b). Immunohistochemistry of  
113 MTO cartilage showed increasing amounts of type II collagen over time as the cartilage matured and  
114 showed extensive expression of aggrecan at all time points (Fig. 1c-d). Type VI collagen was also  
115 extensively expressed in MTO cartilage while Type I collagen showed expression in some sites at the  
116 periphery of MTO cartilage, and Type X collagen generally showed no immunoreactivity above  
117 background (Fig. S2). We noted that the hyaline cartilage phenotype was stably maintained from week 8  
118 to week 30 with prominent growth in size (Fig. 1a-d). To further assess this, we performed  
119 histomorphometric measurements on MTO histologic sections using aggrecan area fraction as a global  
120 indicator of developing and mature cartilage composition of the MTOs. At week 8 (n=7 biological  
121 replicates) the mean aggrecan area fraction was 17.7% ( $\pm$  7.2) and at week 11 (n=5) was 57.8 ( $\pm$  15.1)  
122 with unpaired t-test showing a significant increase from week 8 to 11 (p=0.001) (Fig. 1e).  
123

124 **Fig. 1**



125

126 Histology of 1024 cell line multi-tissue organoids (MTOs) at 8 and 30 weeks, and 9-1 cell line<sup>25</sup> MTOs at

127 11 weeks. **a.** MTOs at 8 weeks shows a developing cartilage nodule with diffuse Alcian blue staining

128 (blue) of the early cartilaginous matrix, diffuse labeling for aggrecan (ACAN, brown) in cells and matrix,

129 and type II collagen labeling (COL2A1, brown) in the cartilaginous matrix of a central region of maturing

130 cartilage. Size bars = 200  $\mu$ m. **b.** MTOs of the 9-1 cell line at 11 weeks show maturing cartilage with

131 increased Alcian blue positive cartilaginous matrix separating chondrocytes, moderate diffuse staining for

132 type II collagen, and diffuse aggrecan labeling. Size bars = 50  $\mu$ m. **c.** 1024 MTOs after 30 weeks in

133 culture show further maturation to hyaline cartilage morphology with chondrocytes surrounded by an

134 abundant matrix with diffuse Alcian blue and type II collagen staining, and pericellular aggrecan staining.

135 Size bars = 50  $\mu$ m. **d.** Low magnification views of 1024 30-week MTOs shown in c. demonstrating the

136 large size attained by some chondrogenic nodules. Measure bar on H&E panel = 4,363  $\mu$ m (4.363 mm).



137 Size bars = 1000  $\mu\text{m}$ . **e.** Histomorphometric measurements on 1024 MTOs histologic sections using  
138 aggrecan area fraction (percentage) in MTOs at week 8 and 11 in 1024 cell line (\*\*\*,  $p=0.001$ ) (Fig. 1e).

139

## 140 Global transcriptome reveals signatures of mesoderm formation in MTOs

141 To understand the transcriptome change underlying the phenotypic development of cartilage in MTOs, we  
142 conducted bulk RNA-seq on 1024-derived MTOs at weeks 8, 11, and 15, which covered the time span  
143 during which our histologic analysis showed emergence, expansion, and maturation of the MTOs  
144 cartilage. Principal component analysis (PCA) of global RNA expression data in MTOs showed distinct  
145 clustering corresponding to the time of collection (Fig. 2a). We conducted differential gene expression  
146 and gene ontology (GO) enrichment of differentially expressed genes for all three comparisons (Fig. S4;  
147 Fig. 2). We were especially interested in the altered expression of several cartilage marker genes at week  
148 15 in comparison to week 8. Likely due to the multi-tissue nature of MTOs, although COL2A1 content  
149 increased in MTOs cartilage (Fig. 1c), it showed decreased expression in bulk RNA-seq. Other cartilage  
150 markers, however, such as *ACAN*, *CD44*, *COMP*, *PRG4*, and *SNAI1*, displayed significantly increased  
151 expression (Fig. 2b; Table S1-2). We note that although transcript levels for collagen type I/X increased,  
152 the expression of another hypertrophic marker, *IHH*, decreased, suggesting that further analyses into  
153 cartilage development pathways were needed. Additionally, type I collagen is the most abundant collagen  
154 and its expression is not limited to cartilage<sup>29</sup>; therefore increased levels of type I collagen transcripts in  
155 MTOs do not necessarily reflect an increase of type I collagen in the composition of MTOs cartilage.  
156 Interestingly, we observed consistent downregulation of neural processes, such as synapse organization  
157 and axonogenesis, and upregulation of mesodermal processes, for example, extracellular matrix  
158 organization, connective tissue development, and cartilage development (Fig. 2c-d; Fig. S4; Table S3-4).

159 Interplays between bone morphogenetic protein (BMP) and fibroblast growth factor (FGF) signaling play  
160 an important and highly conserved role in neural induction and mesoderm patterning, chondrocyte  
161 differentiation, and proliferation, and endochondral ossification during embryonic development studied  
162 almost exclusively in other species<sup>30-33</sup>. We observed a gradual increase in cartilage production from  
163 week 8 to week 15, therefore, we hypothesized that the global neural-to-mesodermal transition observed

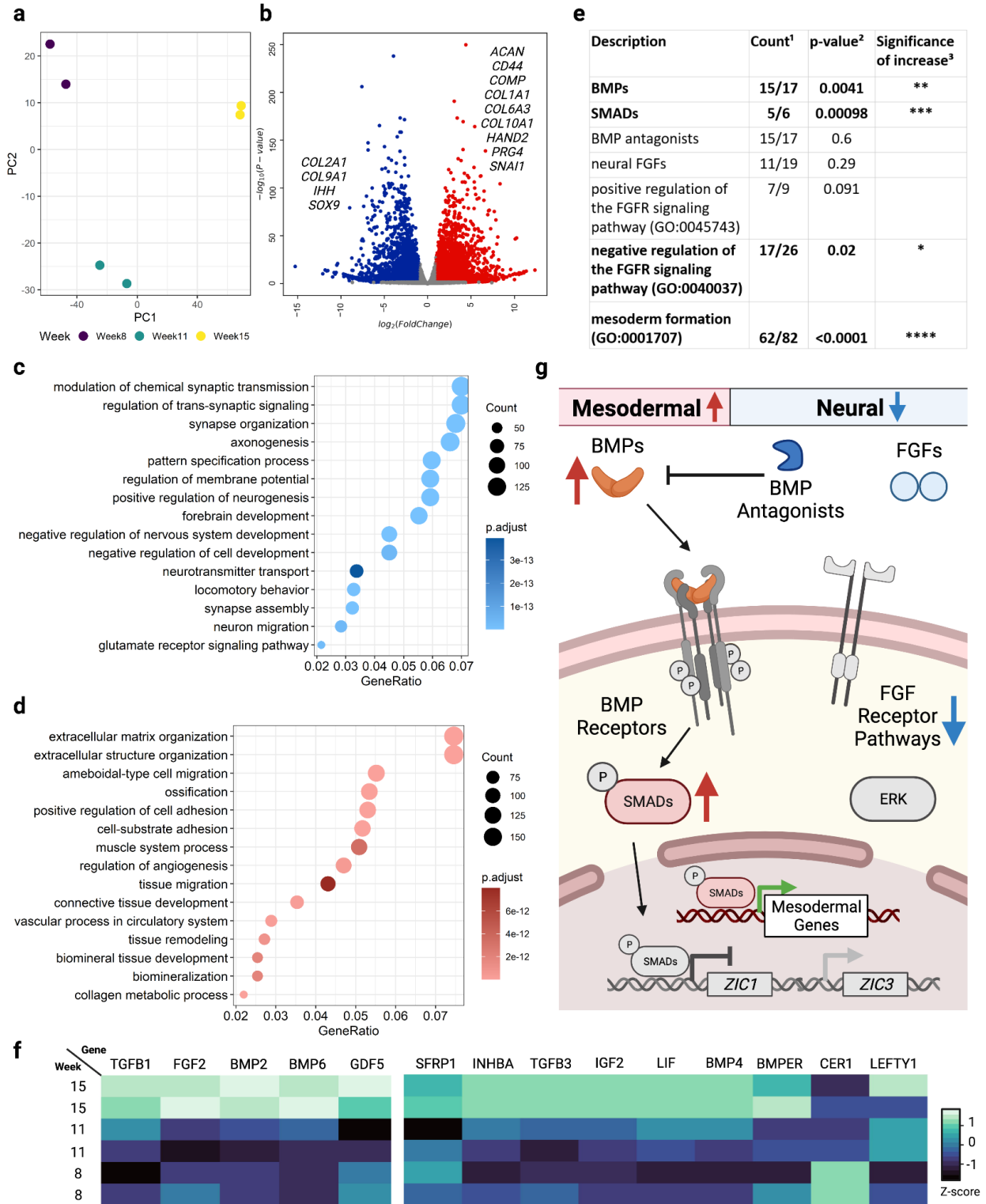
164 in human MTOs would be associated with significantly altered dynamics between BMP and FGF  
165 pathways. Specifically, we expected to see favored BMP pathways, which would entail 1) increased  
166 expression of components in the BMP signaling pathways, 2) reduced or unchanged levels of BMP  
167 antagonists, and 3) reduced or steady levels of FGF signaling. Pathways during mesoderm development  
168 processes are intertwined and expressed in a variety of tissues<sup>30-32</sup>; identifying and examining only a few  
169 expressed genes in one pathway may be biased in bulk-sequencing of MTOs. Therefore, we decided to  
170 examine the expression of genes comprehensively based on previous publications and GO terms and  
171 compared the overall expression of grouped genes between weeks 8 and 15. We observed that there was a  
172 significant increase in the overall expression of BMPs<sup>34</sup> ( $p=0.0041$ ) and their intracellular signaling  
173 transducers—SMADs<sup>34</sup> ( $p=0.00098$ ) (Fig. 2e; Fig. S4a-b). The overall expression of BMP antagonists<sup>35</sup>  
174 remained unchanged ( $p=0.6$ ) (Fig. 2e; Fig. S4c). As for FGF signaling pathways, we first examined the  
175 expression of neural FGFs<sup>36</sup>; which we found to be expressed at lower levels in comparison to other  
176 transcripts described previously although they did not change significantly ( $p=0.29$ ) (Fig 2e; Fig. S4d).  
177 Further, we examined the dynamic expression of other components in the FGFR pathways and observed a  
178 significant increase ( $p=0.02$ ) in negative regulation of the FGFR signaling pathway (GO:0040037) and a  
179 decrease—although not statistically significant ( $p=0.097$ )—in the expression of genes involved in the  
180 positive regulation of the FGFR signaling pathway (GO:0045743) (Fig 2e; Fig. S4e-f). This suggests that  
181 neural FGFs and their downstream pathways were suppressed, agreeing with the observed histological  
182 decrease in neural components. Finally, we investigated the expression dynamics of genes involved in  
183 mesoderm formation (GO:0001707) and we found a significantly increased ( $p<0.0001$ ) expression of  
184 genes involved in this biological process (Fig 2e; Fig. S4g).

185 Because the MTOs spontaneously favored the phenotype of cartilage production without the addition of  
186 chemicals beyond the E8 medium, we wondered if MTOs intrinsically increased the expression of  
187 differentiation factors that are used to induce chondrogenesis. Gene products of *BMP2*, *BMP6*, *FGF2*,  
188 *GDF5*, and *TGFBI*—albeit still being debated—have been suggested to be indispensable for

189 chondrogenesis<sup>5,8</sup>. Interestingly, expression of all of these genes—except *GDF5* (p=0.08)—significantly  
190 increased in MTOs spontaneously from week 8 to week 15 (Fig. 2f; Table S1). In addition, we examined  
191 other genes whose products were used for chondrogenic differentiation in other protocols<sup>6,28</sup>, including  
192 *TGFB3*, *INHBA*, *BMPER*, *BMP4*, *LIF*, *IGF2*, *LEFTY1*, *SFRP1*, and *CER1*. We found that all but *CER1*  
193 displayed increased patterns of expression (Fig. 2f; Table S1). This indicates that molecular mechanisms  
194 underlying spontaneous chondrogenesis in MTOs may resemble those observed in hiPSC-induced  
195 chondrogenic differentiation.

196 Overall, the global transcriptome of hiPSC-derived MTOs showed that increased gene expression in BMP  
197 signaling and mesoderm development, as well as decreased gene expressions in neural FGF signaling  
198 were associated with the increased cartilage production in MTOs from week 8 to week 15 (Fig. 2g).

199 Fig. 2



201 Cartilage development in MTOs is associated with favored BMP signaling pathways and increased  
202 mesodermal gene expression. **a.** Principal component analysis (PCA) of MTO global transcriptomes at  
203 weeks 8, 11, and 15. **b.** Differential gene expression analysis showing differentially expressed cartilage  
204 marker genes between week 8 and week 15. **c.** Ontology enrichment of differentially decreased genes  
205 between week 8 and week 15. **d.** Ontology enrichment of differentially increased genes between week 8  
206 and week 15. **e.** Table displaying the comparison and statistical results of the overall expression of  
207 grouped genes between week 8 and week 15. <sup>1</sup> number of genes expressed/genes associated with the GO  
208 term (retrieved by biomaRt v2.46.3); <sup>2</sup> one-tailed Wilcoxon test comparing normalized and log-  
209 transformed transcript counts between week 8 and week 15; <sup>3</sup> \*, p-value<0.05; \*\*, p-value <0.01, \*\*\*, p-  
210 value <0.001, \*\*\*\*, p-value <0.0001. **f.** Expression of genes in MTOs at weeks 8, 11, and 15 encoding  
211 molecules commonly used for inducing chondrogenesis *in vitro*. **g.** Graphic summary (non-grey objects)  
212 of findings and relevant pathways.

213

214

## 215 Distinct signaling pathways associated with increased articular cartilage 216 development in MTOs

217 The establishment of both cartilage and bone formation is the result of chondrogenesis, which plays an  
218 essential role during the fetal development of the mammalian skeletal system. Hypertrophy of  
219 chondrocytes and deterioration of cartilage matrix precede endochondral ossification that leads to the  
220 formation and growth of long bones<sup>37</sup>. Gene expression for chondrogenesis and ossification overlap  
221 greatly due to the unified nature of cartilage and bone formation. As previously mentioned, we observed  
222 an increase in several cartilage marker genes as well as contradicting expression of *IHH* and *COL10A1* in  
223 the MTOs (Fig 1). Notably, we did not observe the deterioration, mineralization, or osteogenesis of the  
224 cartilage matrix even up to 30 weeks. Therefore, we probed further into the temporal expression patterns  
225 of genes crucial for cartilage development to see if we could identify signaling pathways that may  
226 contribute to the long-term maintenance of chondrocytes. To achieve this, we first investigated gene  
227 expression under the GO term cartilage development (GO:0051216) which includes both the positive and  
228 negative regulators of cartilage development<sup>35</sup>. We visualized the expression pattern of 125 (FDR<0.05)  
229 out of the 194 genes retrieved by biomaRt and found a clear separation of 42 and 83 genes with decreased  
230 and increased expression, respectively (Fig. 3a)<sup>38</sup>. In addition, despite the decrease of 42 genes, the  
231 overall gene expression levels increased significantly ( $p<0.0001$ ) for cartilage development (Fig. 3a),  
232 agreeing with the expansion of cartilage in MTOs. We hypothesized that there would be distinct  
233 interactions of gene products between selected genes with increased and decreased expression. Therefore,  
234 we used STRING to construct two functional association networks consisting of proteins expressed by the  
235 described genes. Transcription factors and growth factors were the most connected molecules for both  
236 networks. Interestingly, we found that Wnt signaling molecules constituted the most prominent local  
237 network clusters in the network cluster organization for decreased gene products (Fig. 3b; Table 1; Table  
238 S5-6). Wnt signaling cascades have essential roles in the development and homeostasis of chondrogenesis  
239 and ossification<sup>39</sup>. In general, canonical Wnt cascades—including ROR2 and SFRP2 highlighted in the

240 network—inhibits the early stages of chondrogenesis<sup>38</sup>. *WNT7A* overexpression blocked early  
241 chondrogenesis in chick limb model<sup>40</sup>. During endochondral ossification, Wnt signaling pathways  
242 promote chondrocyte hypertrophy<sup>39</sup>. *SFRP2*, *WNT01B*, and *WNT7B* are known positive regulators of  
243 ossification<sup>35</sup> (Fig. 3a). Additionally, some non-Wnt positive regulators of ossification were also  
244 downregulated. Among the upregulated members, we observed clusterings centered on TGF-beta/BMP  
245 signaling pathways (Fig 3c; Table 1; Table S5-6). This is not surprising given TGF-beta/BMP signaling  
246 pathways predominantly promote all stages of chondrogenesis<sup>41,42</sup>. We also found a unique signature of  
247 increased downregulation of the canonical Wnt signaling pathway, agreeing with the association network  
248 formed by protein products of genes with decreased expression. In contrast to the previous network, we  
249 observed that several negative regulators of ossification mostly did not overlap with TGF-beta/BMP  
250 signaling pathways (Fig. 3c; Fig. S4). In summary, from week 8 to week 15, the cartilage in MTOs was  
251 likely stably growing due to continued increase in TGF-beta/BMP pathways promoting chondrogenesis  
252 and downregulation of Wnt signaling cascades that inhibit chondrocyte hypertrophy and ossification in  
253 maturing chondrocytes.

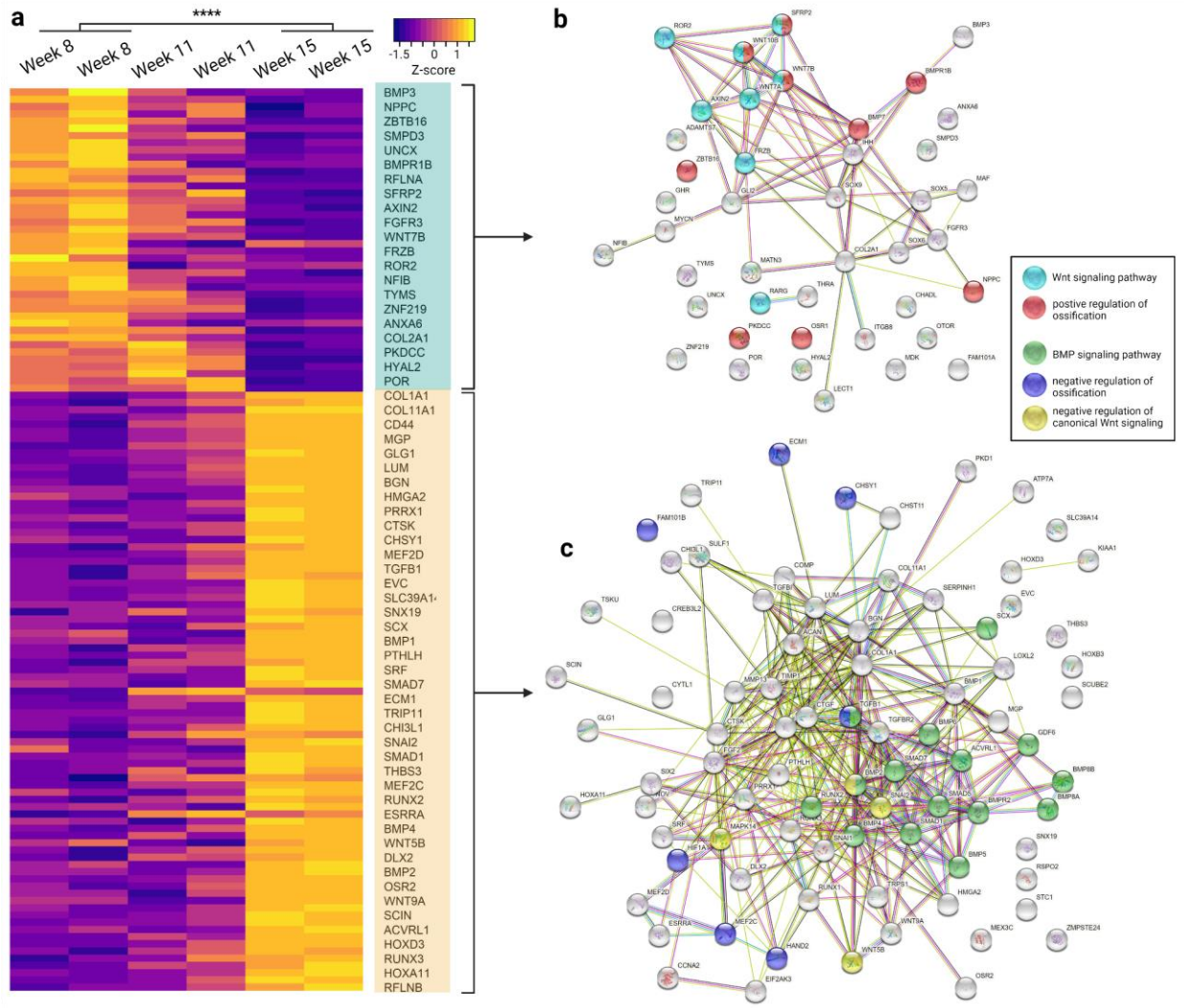
254 In addition, we also compared the expression of genes for biological processes of interest as described  
255 above (Table 2; Table S7) using GO term gene lists retrieved by biomaRT from GO to reduce bias in  
256 gene selection<sup>35</sup>. Again, we found that genes in GO terms associated with promoting cartilage maturation,  
257 including positive regulation of cartilage development (GO:0061036), chondroblast differentiation  
258 (GO:0060591), and cartilage morphogenesis (GO:0060536), demonstrated significantly increased  
259 expression (Table 2; Table S7), while growth plate cartilage development gene set (GO:0003417) was not  
260 significantly increased ( $p=0.058$ ). Moreover, the expression of genes associated with negative regulation  
261 of chondrocyte maturation and promotion of endochondral ossification did not show significant changes  
262 (Table 2; Table S7). As we observed the marginally insignificant increase of growth plate cartilage  
263 development (GO:0003417) marker gene expression ( $p=0.058$ ), we wondered if the growth in hyaline  
264 cartilage produced by MTOs would be more closely associated with the increased expression of articular



265 cartilage gene markers but not others. Indeed, we only observed a significant increase in the expression of  
266 articular cartilage marker genes (GO:0061975; p=0.031) and not bronchus or trachea cartilage  
267 development (GO:0060532; GO:0060534).

268 To summarize, we observed that protein products of genes with decreased expression in MTOs from  
269 week 8 to week 15 were clustered around components of Wnt signaling pathways that promote  
270 ossification while those with increased expression formed prominent networks around TGF-beta/BMP  
271 signaling pathways. Moreover, the observed molecular signaling clusters were associated with a unique  
272 increase in the gene expression of articular cartilage development.

273 **Fig. 3**



274

275 Cartilage development in MTOs is associated with distinct Wnt and TGF-beta/BMP signaling. **a.** 125  
 276 genes were selected (FDR<0.05) and their scaled temporal expression at weeks 8, 11, and 15 were  
 277 plotted; genes were arranged by decreased and increased expression. Gene expression between week 8  
 278 and week 15 was compared. \*\*\*\*, p<0.0001. **b.** Functional association network of protein production  
 279 expressed by genes with decreased expression. **c.** Functional association network of protein production  
 280 expressed by genes with increased expression.

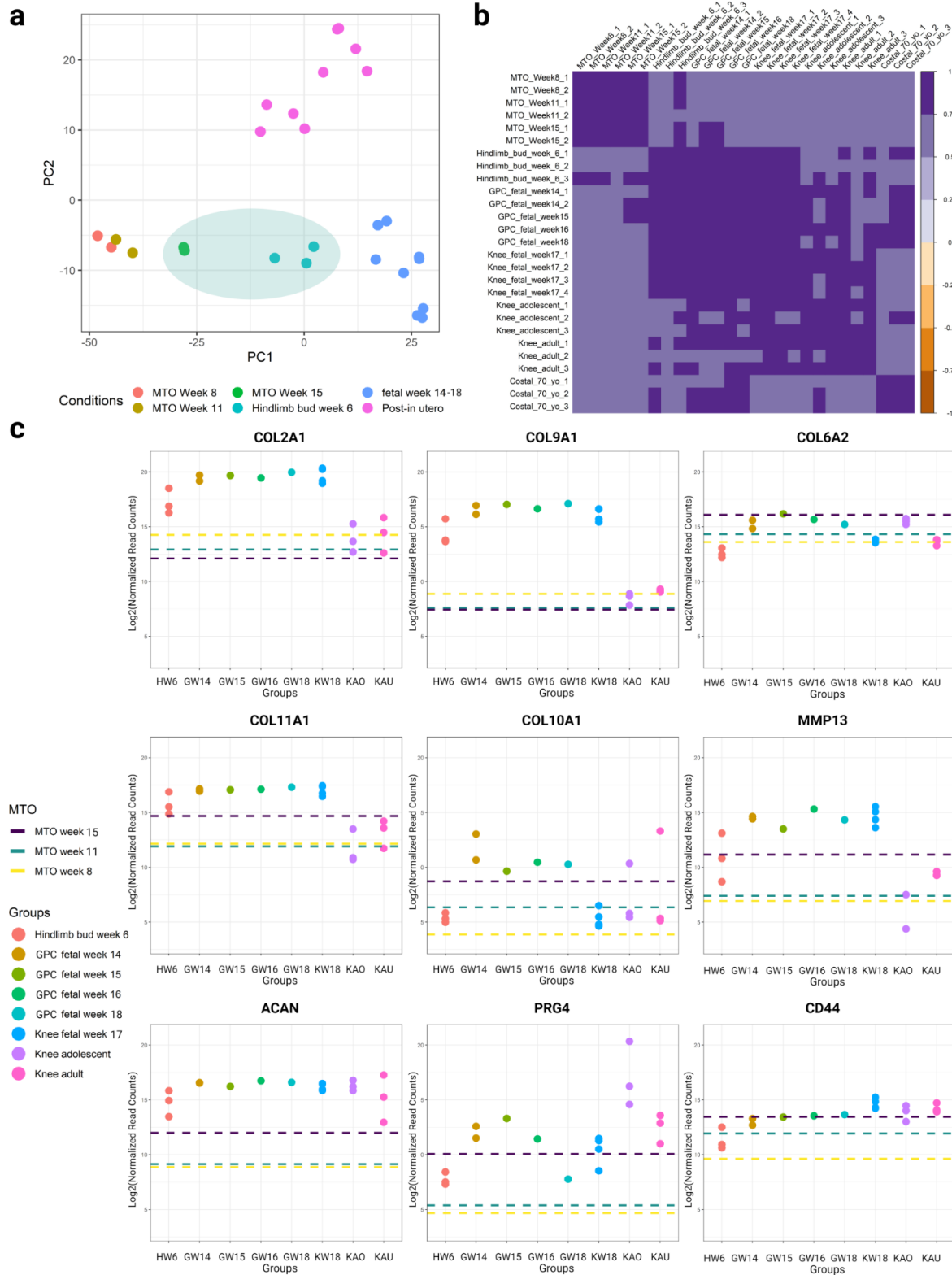
281 Transcriptomic comparisons between MTOs and lower limb chondrocytes cross  
282 human life stages

283 Because MTO RNA-seq revealed a unique increase in articular cartilage development, we hypothesized  
284 that there would be a strong correlation between MTOs and human growth plate chondrocytes and/or  
285 articular chondrocytes in the expression of genes specific to chondrocytes<sup>26</sup>. We first reprocessed existing  
286 RNA-Seq data collected from human embryonic limb bud (week 6)<sup>26</sup>, growth plate chondrocytes (week  
287 14, 15, 16, and 18)<sup>26</sup>, knee chondrocytes (week 17, adolescent, and adult)<sup>27,28</sup>, as well costal chondrocytes  
288 (~70-year-old adults)<sup>6</sup>. We validated 325 genes known to be specifically expressed by chondrocytes<sup>26</sup>; we  
289 conducted PCA on these genes and found that the effect of different studies is minimal as gene expression  
290 was clustered by life stages rather than particular studies (Fig. 4a). Specifically, fetal tissues (growth plate  
291 and knee chondrocytes) clustered together while cartilage tissues from adolescents, adults, and 70-year-  
292 olds (knee and costal chondrocytes)—collectively addressed as post-*in utero* tissues—located in close  
293 proximity to each other (Fig. 4a). We highlight that 15-week MTOs were most similar to 6-week human  
294 limb bud cartilaginous tissues (Fig. 4a). Then, we used the Pearson correlation coefficient to examine the  
295 correlation among all samples and genes included in the PCA analysis. Agreeing with previous GO  
296 analysis and PCA, while all MTOs showed >60% correlation with human chondrocytes and cartilage  
297 tissues from all life stages, 15-week MTOs showed an even stronger correlation (>76%) with 6-week  
298 human limb bud and 14-week and 15-week fetal growth plate chondrocytes (Fig. 4b; Table S9).  
299 Moreover, we found that MTOs, on average for previously described genes of  
300 interest, showed a significantly higher ( $p < 0.0001$ ; 95% CI [0.053,  $+\infty$ ])  
301 correlation with fetal chondrocytes than post-*in utero* knee chondrocytes; the  
302 average correlation between MTOs and fetal tissues was 71% while that for post-*in utero* tissues was  
303 65%.

304 We further examined the expression of known collagen genes (*COL2A1*, *COL9A1*, *COL6A2*, *COL11A1*,  
305 *COL10A1*)<sup>43</sup>, hypertrophic markers (*COL10A1*, *MMP13*), and some components reflecting the secretory  
306 functions of chondrocytes (*ACAN*, *CD44*, *PGR4*) in MTOs as compared to human lower limb  
307 chondrocytes. We found that transcripts of components for ECM were generally more abundant from *in*  
308 *utero* than post-*in utero* lower limb chondrocytes, while those for secretory molecules showed more  
309 variable trends. Although the expression of genes encoding for type 2/9 collagen (*COL2A1*, *COL9A1*)  
310 was lower in 15-week MTOs, the expression from 8- and 11-week MTOs fell in the range defined by  
311 examined human tissues. The expression of other major collagen components making up the non-  
312 hypertrophic region of cartilage (*COL6A2* and *COL11A1*) and hypertrophic markers (*COL10A1*, *MMP13*)  
313 were not noticeably different between MTOs and human lower limb cartilaginous tissues. Among MTOs  
314 collected at different time points, despite falling in expression ranges of human tissues, 15-week MTOs  
315 showed slightly lower collagen contents and higher hypertrophic gene expression. As for transcripts of  
316 secretory molecules, 15-week MTOs showed similar expression (*PGR4*, *CD44*) to human tissues except  
317 for lower *ACAN*. We note that the normal expression of *PRG4*, a gene encoding for a large proteoglycan  
318 synthesized by chondrocytes located at the surface of articular cartilage and by some synovial lining  
319 cells<sup>44</sup>, offers additional support to the articular developmental trajectory spontaneously taken by MTO  
320 chondrocytes. In short, we found that transcripts levels of genes specifically expressed in human growth  
321 plate chondrocytes were strongly correlated between 15-week MTOs and human lower limb cartilaginous  
322 tissues.

323

324 Fig. 4



325

326 Transcription signatures in MTOs are comparable with human lower limb chondrocytes. **a.** Principal  
327 component analysis (PCA) on 325 chondrocyte-specific genes in MTOs and human lower limb  
328 chondrocytes. **b.** Pearson correlation plot of 325 chondrocyte-specific genes in MTOs and human lower  
329 limb chondrocytes. **c.** Representative comparisons of marker transcripts (*COL2A1*, *COL9A1*, *COL6A2*,  
330 *COL11A1*, *COL10A1*, *MMP13*, *ACAN*, *CD44*, *PGR4*) in MTOs and human lower limb chondrocytes.  
331 MTOs, multi-tissue organoids; GPC, growth plate chondrocytes.

## 332 **Discussion**

---

333 Chondrogenesis and hyaline cartilage production *in vitro* is needed to provide chondrocytes for cartilage  
334 regenerative therapies as well as for *ex vivo* OA modeling. Despite recent advances in hiPSC-based *in*  
335 *vitro* chondrogenesis<sup>5,6</sup>, the development of simple and scalable protocols to generate chondrocytes for  
336 therapeutic purposes as well as the understanding of dynamic cell behaviours in long-term cultures are yet  
337 to be accomplished. Here, we report the spontaneous emergence and robust growth of hyaline cartilage in  
338 hiPSC-derived MTOs grown in xeno- and feeder-free, chemically-defined cultures, making this protocol  
339 amenable for clinical good manufacturing practices (cGMP). Furthermore, the relative technical  
340 simplicity of the process also makes it suitable for robotic cell culture and scaled-up manufacturing. By  
341 characterizing and analyzing the transcriptome changes during the phenotypic transition of MTOs, we  
342 provide a mechanistic foundation for future organoid and related tissue engineering aiming at rapid  
343 cartilage production to thrive upon.

344 We first described the morphology and characteristic histochemical and immunohistochemical features of  
345 the MTO-cartilage. Specifically, prominent hyaline cartilage emerged by week 8 of culturing MTOs and  
346 continued to expand in size. Further, we found that COL2A1 IHC staining increased over time as the  
347 cartilage matured despite decreased transcript level, Type VI collagen was present especially in  
348 pericellular locations, while COL1A1 showed restricted immunoreactivity most evident at the periphery  
349 of cartilage at the junction with surrounding tissue, and COL10A1 was generally not detectable above  
350 background. We conclude that the hyaline cartilage produced by MTOs is most similar to articular  
351 hyaline cartilage. Key collagen and ECM compositions affect the functional performance of cartilages.  
352 Cartilage with greater tensile strength contains a higher content of collagen type II/IX, aggrecan, and a  
353 lower content of collagens type I/X<sup>45-47</sup>. Higher aggrecan content in the ECM allows more capacity for  
354 the cartilage to withstand compression<sup>45-47</sup>. Our findings, therefore, suggest that MTO cartilage will have  
355 biomechanical properties similar to articular cartilage including resistance to repetitive forces of  
356 compression and shear.

357 MTOs were formed by the previously reported CO<sup>25</sup> undergoing a substantial and self-organized  
358 transition without interventions beyond the change of flask and regular media change. In contrast to the  
359 increase in neural cells in hiPSC-derived chondrocyte populations observed by Wu et al<sup>6</sup>, we observed a  
360 consistent decrease in neural lineages in MTOs collected at different time points. It is unclear whether  
361 cells of neural lineages during MTO development underwent senescence or fate switching. Regardless,  
362 neural crest cells (NCC) may have emerged from neural tube-like structures present in CO, which later  
363 spontaneously formed mesodermal derivatives, such as chondrocytes. Induction of chondrocytes from  
364 hiPSC through NCC intermediates has been recently reported by two independent groups<sup>5,7</sup>. Moreover,  
365 RNA-seq of MTOs agreed with the phenotypic transition of MTOs from week 8 to week 15, where we  
366 observed favored BMP pathway signaling and increased mesodermal processes associated with cartilage  
367 production. Interestingly, MTOs showed spontaneous increases in the expression of all genes coding for  
368 previously reported inductive factors essential for chondrogenesis, including *BMP2*, *BMP6*, *FGF2*,  
369 *GDF5*, and *TGFBI*<sup>5,8</sup>; this suggests that MTO chondrocytes likely shared similar, albeit spontaneous,  
370 developmental trajectories with other hiPSC-derived chondrocytes<sup>5,8</sup>. Together, although our data only  
371 demonstrated correlative relationships, existing literature surrounding chondrogenic differentiation and  
372 the conserved roles of BMP and FGF signaling pathways suggests that favored expression of components  
373 in BMP signaling pathways resulted in the increased cartilage production in MTOs. This was further  
374 supported by the prominent clustering of TGF-beta/BMP signaling pathways formed by gene products  
375 encoded by genes with increased expression during cartilage development in MTOs. Furthermore, we  
376 observed a probable downregulation of components in the Wnt signaling pathways related to cartilage  
377 development. This is in agreement with previous reports indicating that Wnt signaling pathways inhibit  
378 chondrogenesis and/or promote ossification<sup>39,48,49</sup>. With regard to hiPSC-derived chondrocytes, Wnt  
379 signaling was recently shown to cause off-target differentiation during chondrogenesis by Wu et al<sup>6</sup>. We  
380 were not surprised to see the overlaps of ossification and TGF-beta/BMP pathways because markers for  
381 cartilage development—such as *BMP2* and *BMP6*—are largely expressed throughout the hypertrophic  
382 change of chondrocytes<sup>34</sup>. Therefore, the increase in TGF-beta/BMP pathways involved in ossification



383 should not be solely interpreted as progress towards ossification. This was further supported by the non-  
384 significant change in expression of genes involved in chondrocyte differentiation associated with  
385 endochondral bone morphogenesis (GO:0003413). To summarize, it is likely that 1) the favoring of BMP  
386 signaling pathways over neural FGF pathways promoted mesoderm formation and 2) the combination of  
387 upregulated TGF-beta/BMP signaling and downregulated Wnt signaling components resulted in the long-  
388 term maintenance of cartilage growth and its specific increase expression of articular cartilage  
389 development marker genes. Our findings did not, however, rule out the involvement of other pathways or  
390 the differential signaling within a subset of pathways. For example, the crosstalk between canonical and  
391 noncanonical TGF-beta signaling pathways may also contribute to the maintenance of cartilage<sup>50</sup> in  
392 MTOs. Extensive research to understand and manipulate the precise spatiotemporal expression of  
393 aforementioned components during MTO development, specifically in chondrocytes and their precursors,  
394 would be needed to establish definitive causative effects. MTOs may serve as human-specific models for  
395 disease modeling and drug testing due to the developmental dynamics of key chondrogenic pathways.

396 To evaluate the similarities and differences between cartilage<sup>51</sup> from MTOs and human tissues, we  
397 reprocessed existing RNA-Seq data obtained from human fetal limb bud, and chondrocytes from fetal  
398 growth plate and knee, and adolescent and adult chondrocytes. We found that the 15-week MTOs showed  
399 a strong correlation (>76%) with human fetal limb bud and growth plate chondrocytes for growth plate  
400 chondrocyte-specific gene expression. Together with comparable levels of *PRG4* transcripts, the result  
401 suggests that MTOs spontaneously adopt the trajectory of articular cartilage development during long-  
402 term culture. Although there is a slight difference in the expression of type II/IX collagen transcripts, the  
403 expression of other cartilage components and secretory chondrocyte molecules were similar. The  
404 expression of collagen contents in MTOs may change and/or improve as the environment becomes more  
405 physiological. Long-term implantation of chondrocytes in large animals may shed light on the therapeutic  
406 value of MTO-derived chondrocytes.

407 To conclude, the long-term culture of hiPSC-derived MTOs results in the spontaneous emergence of  
408 mesoderm-derived articular cartilaginous tissues and the MTO cartilage resembles fetal limb bud and  
409 growth plate chondrocytes. Despite previous reports of hyaline cartilage appearance facilitated by  
410 chondrogenic induction of hiPSC *in vitro*<sup>5-8</sup>, MTO-generated cartilage stands out as they are larger, more  
411 mature, and can be maintained in long-term cultures. This process was also self-organized with a  
412 comparably simpler, xeno- and feeder-free, 3D culturing protocol, making production easily adaptable to  
413 cGMP production and amenable to scaled-up commercial manufacturing. The transition from CO  
414 ectodermal trajectory to the commitment of articular cartilage development in MTOs reported here further  
415 illustrates the remarkable self-organization capability of organoids.

416

417

## 418 **Methods**

---

### 419 **Generating hiPSC-derived multi-tissue organoids (MTOs)**

420 iPSC lines referred to as 1024 (ATCC-BYS0110, Cat. #ACS-1024) and 9-1 (UMN PCBC16iPS/vShiPS  
421 9-1)<sup>25</sup> were expanded in culture on vitronectin (VTN-N, ThermoFisher Scientific, Cat. #A14700) in  
422 Essential 8 Medium (E8, Thermo Fisher Scientific Life Sciences). iPSCs were harvested using sodium  
423 citrate buffer, briefly centrifuged, and MTO induction initiated by resuspension in 40  $\mu$ L of the fluid of  
424 hydration from Cell-Mate3D  $\mu$ Gel 40 Kit (BRTI Life Sciences, Two Harbors, MN, USA) which was then  
425 transferred to one well of a 6-well ultra-low attachment plate (Costar™ Ultra-Low Attachment  
426 Microplates, Corning Life Sciences, Corning, NY, USA) containing 5 ml of E8 medium and incubated for  
427 24 hrs. Cells and culture medium were then transferred to a G-Rex 100 bioreactor (Wilson Wolf, New  
428 Brighton, MN) and incubated at 37°C in 5% CO<sub>2</sub>. E8 culture medium containing 1% antibiotic-  
429 antimycotic (Gibco Thermo Fisher Scientific) was changed every 3-4 days over the entirety of MTO  
430 culture.

### 431 **Histology and Immunohistochemistry**

432 MTOs were harvested on weeks 8 and 11 (both cell lines) and week 30 (1024 only), placed in 10%  
433 neutral buffered formalin solution and fixed at room temperature for 3.5 hours. After fixation, samples  
434 were transferred to 70% ethanol solution until they were processed for routine paraffin embedding.  
435 Samples were then sectioned 4- $\mu$ m thick, deparaffinized, rehydrated, and routinely stained with  
436 hematoxylin and eosin (H&E) and Alcian blue. For immunohistochemical staining, sections were cut at 4  
437  $\mu$ m, deparaffinized, and rehydrated, followed by incubation with 3% hydrogen peroxide to quench  
438 endogenous peroxidase activity and 15 minutes in serum-free protein block (DAKO, Glostrup, Denmark).  
439 Sections were then subjected to appropriate antigen retrieval methods (if needed) and incubated with the  
440 primary antibody at room temperature for 60 minutes (Table S10). Color development was done using  
441 EnVision FLEX DAB+ substrate chromogen system (Cat.# GV825, Agilent-Dako, Santa Clara, CA,

442 USA). Stained sections were examined with an Olympus BH-2 microscope (Olympus America, Center  
443 Valley, PA) and imaged with a SPOT Insight 4 megasample digital camera and SPOT Advanced software  
444 (Diagnostic Instruments Inc., Sterling Heights, MI).

## 445 Morphometry

446 Aggrecan IHC stained histologic sections of MTO biological replicates at 8 weeks (n=7) and 11 weeks  
447 (n=5) were analyzed for aggrecan staining area fraction (staining area/total area of tissue) using a Nikon  
448 Eclipse E-800M bright field/fluorescence/dark field microscope equipped with a Nikon DXM1200 high-  
449 resolution digital camera. Images for histomorphometry were analyzed using ImageJ2/Fiji software  
450 (National Institutes of Health, open-source). Values are reported as area fraction (%)  $\pm$  standard deviation.

## 451 RNA-seq of MTOs and data generation

452 MTOs were disaggregated into single cell or small clusters to enhance RNA extraction. MTOs were  
453 pipetted from the bioreactor, rinsed in PBS and suspended in 2 ml trypsin (0.025%, Sigma Aldrich) for 2  
454 minutes at 37°C. Next, a scalpel was used to mechanically disrupt the MTOs in a conical tube in 600  $\mu$ g  
455 DNase1 in an additional 3 ml of 0.025% trypsin and this was incubated for 5 minutes at 37°C. MTOs  
456 were then dissociated by a stream of cold Hank's Balanced Salt Solution (HBSS; Life Technologies) over  
457 a 100  $\mu$ m filter (BD Biosciences, San Jose, CA). Organoid tissue retained on the filter was then back-  
458 flushed with 25 ml of cold HBSS and this tissue was further disaggregated in 2 ml Collagenase II (Celase  
459 GMP, Worthington Biochemical Corporation, Lakewood, NJ) also containing 200  $\mu$ g DNase1, for 5  
460 minutes at 37°C. After incubation, tissue was gently triturated with a 5 ml pipet and an additional 3 ml of  
461 Collagenase II with 300  $\mu$ g DNase1 added, and this preparation was incubated for 5 minutes at 37°C.  
462 The cells were then centrifuged at 350 x g for 3 minutes at 4°C, the cell pellet was resuspended in cold  
463 HBSS, centrifuged again and resuspended in HBSS.

464 The MTO cell preparations were then lysed in RLT buffer (Qiagen, Hilden, Germany) and RNA isolated  
465 from cell lysates using the RNeasy Plus mini kit (Cat. No. / ID: 74134Qiagen, Hilden, Germany)  
466 according to the manufacturer's instructions. Extracted RNA was then quantified by RiboGreen RNA  
467 assay (Thermo Fisher Scientific, Waltham, MA) and quality/size analyzed by Agilent BioAnalyzer  
468 (Agilent Technologies, Santa Clara, CA). 2 x 50bp FastQ paired-end reads for 6 samples (n=62.4 Million  
469 average per sample) were trimmed using Trimmomatic (v0.33) enabled with the optional "-q" option; 3bp  
470 sliding-window trimming from 3' end requiring minimum Q30. Quality control on raw sequence data for  
471 each sample was performed with FastQC. Read mapping was performed via Hisat2 (v2.1.0) using the  
472 Human genome (GRCh38) as reference. Gene quantification was done via Feature Counts for raw read  
473 counts. Existing RNA-seq data were processed using the same pipeline.

#### 474 RNA-seq data analysis

475 Raw read counts (CPM) were used as input for differentially expressed genes (DGE) analysis by DESeq2  
476 package (v1.30.1) in R (v4.0.5)<sup>52</sup>. P-values were adjusted (p-adj) using Benjamini-Hochberg correction.  
477 The significant term was determined by using a cut-off of 0.05 (FDR corrected  $p < 0.05$ ) and minimum 2x  
478 Absolute Fold Change. TopGo package (v2.42.0)<sup>53</sup> was used to carry out ontology enrichment of DGE  
479 results<sup>35</sup>. Enrichment results were visualized using ClusterProfiler (v3.18.1)<sup>54</sup>. Cut-offs for p-value (after  
480 applying the Benjamini-Hochberg correction) and q-value were 0.05 and 1, respectively. Genes with  
481 expression  $FDR < 0.05$  were selected and uploaded to STRING (v11) was used for functional protein  
482 association networks for probable gene products; Euclidean distances were used to cluster gene  
483 products<sup>55</sup>. Local network clusters were downloaded from STRING analysis<sup>55</sup>.

#### 484 Additional statistical information

485 The one-tailed Welch's t-test was used to compare histomorphometric measurements on MTO histologic  
486 sections. P-value was reported ( $\alpha = 0.05$ ). Two biological replicates for MTOs were used for RNA-Seq. All

487 gene expression data used for visualization and statistical tests were first normalized and transformed  
488 using `rlog()` and `assay()` in DESeq2<sup>52</sup>. The one-tailed Wilcoxon signed-rank test was used to acquire  
489 statistical results for the change in expression of grouped genes; p-values were reported ( $\alpha=0.05$ ). The  
490 one-tailed pairwise t-test was used to compare the expression of single genes; p-values were reported  
491 ( $\alpha=0.05$ ). Confidence intervals were reported when applicable.

492

493

## 494 **Data Availability**

---

495 All RNA-seq data and raw read counts generated for the analyses herein are publically available within  
496 the NCBI SRA archive under project number: GSE184007.

## 497 **References**

- 498 1. Dewan, A. K., Gibson, M. A., Elisseeff, J. H. & Trice, M. E. Evolution of autologous chondrocyte  
499 repair and comparison to other cartilage repair techniques. *Biomed Res. Int.* **2014**, 272481 (2014).
- 500 2. Francis, S. L., Di Bella, C., Wallace, G. G. & Choong, P. F. M. Cartilage Tissue Engineering Using  
501 Stem Cells and Bioprinting Technology—Barriers to Clinical Translation. *Frontiers in Surgery* vol.  
502 5 70 (2018).
- 503 3. Huang, H., Xu, H. & Zhang, J. Current Tissue Engineering Approaches for Cartilage Regeneration.  
504 in *Cartilage Tissue Engineering and Regeneration Techniques* 13 (IntechOpen Limited, 2019).
- 505 4. Koyama, N. *et al.* Human Induced Pluripotent Stem Cells Differentiated into Chondrogenic Lineage  
506 Via Generation of Mesenchymal Progenitor Cells. *Stem Cells Dev.* **22**, 102–113 (2012).
- 507 5. Lee, M. S. *et al.* Comparative evaluation of isogenic mesodermal and ectomesodermal chondrocytes  
508 from human iPSCs for cartilage regeneration. *Science Advances* **7**, eabf0907 (2021).
- 509 6. Wu, C. L. *et al.* Single cell transcriptomic analysis of human pluripotent stem cell chondrogenesis.  
510 *Nat. Commun.* **12**, 362 (2021).
- 511 7. Yoshimatsu, M. *et al.* In vivo regeneration of rat laryngeal cartilage with mesenchymal stem cells  
512 derived from human induced pluripotent stem cells via neural crest cells. *Stem Cell Res.* **52**, 102233  
513 (2021).
- 514 8. Yamashita, A. *et al.* Generation of Scaffoldless Hyaline Cartilaginous Tissue from Human iPSCs.  
515 *Stem Cell Reports* **4**, 404–418 (2015).
- 516 9. Lach, M. S. *et al.* Chondrogenic differentiation of pluripotent stem cells under controllable serum-  
517 free conditions. *Int. J. Mol. Sci.* **20**, (2019).
- 518 10. Crispim, J. F. & Ito, K. De novo neo-hyaline-cartilage from bovine organoids in viscoelastic

- 519 hydrogels. *Acta Biomater.* **128**, 236–249 (2021).
- 520 11. Kim, J., Koo, B. K. & Knoblich, J. A. Human organoids: model systems for human biology and  
521 medicine. *Nat. Rev. Mol. Cell Biol.* **21**, 571–584 (2020).
- 522 12. Rossi, G., Manfrin, A. & Lutolf, M. P. Progress and potential in organoid research. *Nat. Rev. Genet.*  
523 **19**, 671–687 (2018).
- 524 13. Camp, J. G. *et al.* Human cerebral organoids recapitulate gene expression programs of fetal  
525 neocortex development. *Proceedings of the National Academy of Sciences* **112**, 15672–15677  
526 (2015).
- 527 14. Amiri, A. *et al.* Transcriptome and epigenome landscape of human cortical development modeled in  
528 organoids. *Science* **362**, eaat6720 (2018).
- 529 15. Kanton, S. *et al.* Organoid single-cell genomic atlas uncovers human-specific features of brain  
530 development. *Nature* **574**, 418–422 (2019).
- 531 16. Tanaka, Y., Cakir, B., Xiang, Y., Sullivan, G. J. & Park, I.-H. Synthetic Analyses of Single-Cell  
532 Transcriptomes from Multiple Brain Organoids and Fetal Brain. *Cell Rep.* **30**, 1682–1689 (2020).
- 533 17. Jourdon, A., Scuderi, S., Caputo, D., Abyzov, A. & Vaccarino, F. M. PsychENCODE and beyond:  
534 transcriptomics and epigenomics of brain development and organoids. *Neuropsychopharmacology*  
535 **46**, 70–85 (2021).
- 536 18. Sridhar, A. *et al.* Single-Cell Transcriptomic Comparison of Human Fetal Retina, hPSC-Derived  
537 Retinal Organoids, and Long-Term Retinal Cultures. *Cell Rep.* **30**, 1644–1659 (2020).
- 538 19. Combes, A. N., Zappia, L., Er, P. X., Oshlack, A. & Little, M. H. Single-cell analysis reveals  
539 congruence between kidney organoids and human fetal kidney. *Genome Med.* **11**, 3 (2019).
- 540 20. Guiu, J. *et al.* Tracing the origin of adult intestinal stem cells. *Nature* **570**, 107–111 (2019).
- 541 21. Turco, M. Y. *et al.* Trophoblast organoids as a model for maternal–fetal interactions during human  
542 placentation. *Nature* **564**, 263–267 (2018).
- 543 22. Hardingham, T. & Bayliss, M. Proteoglycans of articular cartilage: Changes in aging and in joint  
544 disease. *Semin. Arthritis Rheum.* **20**, 12–33 (1990).



- 545 23. Herberts, C. A., Kwa, M. S. G. & Hermsen, H. P. H. Risk factors in the development of stem cell  
546 therapy. *J. Transl. Med.* **9**, 29 (2011).
- 547 24. Halme, D. G. & Kessler, D. A. FDA Regulation of Stem-Cell–Based Therapies. *N. Engl. J. Med.*  
548 **355**, 1730–1735 (2006).
- 549 25. Lindborg, B. A. *et al.* Rapid Induction of Cerebral Organoids From Human Induced Pluripotent  
550 Stem Cells Using a Chemically Defined Hydrogel and Defined Cell Culture Medium. 694–702  
551 (2016).
- 552 26. Li, B., Balasubramanian, K., Krakow, D. & Cohn, D. H. Genes uniquely expressed in human growth  
553 plate chondrocytes uncover a distinct regulatory network. *BMC Genomics* **18**, 983 (2017).
- 554 27. Hicks, M. R. *et al.* ERBB3 and NGFR mark a distinct skeletal muscle progenitor cell in human  
555 development and hPSCs. *Nat. Cell Biol.* **20**, 46–57 (2018).
- 556 28. Ferguson, G. B. *et al.* Mapping molecular landmarks of human skeletal ontogeny and pluripotent  
557 stem cell-derived articular chondrocytes. *Nat. Commun.* **9**, (2018).
- 558 29. Henriksen, K. & Karsdal, M. A. Chapter 1 - Type I Collagen. in *Biochemistry of Collagens,*  
559 *Laminins and Elastin* (ed. Karsdal, M. A.) 1–11 (Academic Press, 2016).
- 560 30. Marchal, L., Luxardi, G., Thomé, V. & Kodjabachian, L. BMP inhibition initiates neural induction  
561 via FGF signaling and *Zic* genes. *Proc. Natl. Acad. Sci. U. S. A.* **106**, 17437–17442 (2009).
- 562 31. Aruga, J. & Mikoshiba, K. Role of BMP, FGF, calcium signaling, and *zic* proteins in vertebrate  
563 neuroectodermal differentiation. *Neurochem. Res.* **36**, 1286–1292 (2011).
- 564 32. Schliermann, A. & Nickel, J. Unraveling the Connection between Fibroblast Growth Factor and  
565 Bone Morphogenetic Protein Signaling. *Int. J. Mol. Sci.* **19**, 3220 (2018).
- 566 33. Tani, S., Chung, U.-I., Ohba, S. & Hojo, H. Understanding paraxial mesoderm development and  
567 sclerotome specification for skeletal repair. *Exp. Mol. Med.* **52**, 1166–1177 (2020).
- 568 34. Wang, R. N. *et al.* Bone Morphogenetic Protein (BMP) signaling in development and human  
569 diseases. *Genes and Diseases* **1**, 87–105 (2014).
- 570 35. Carbon, S. *et al.* The Gene Ontology resource: Enriching a GOld mine. *Nucleic Acids Res.* **49**, 325–

- 571 334 (2021).
- 572 36. Ornitz, D. M. & Itoh, N. The fibroblast growth factor signaling pathway. *Wiley Interdiscip. Rev.*  
573 *Dev. Biol.* **4**, 215–266 (2015).
- 574 37. DeLise, A. M., Fischer, L. & Tuan, R. S. Cellular interactions and signaling in cartilage  
575 development. *Osteoarthritis Cartilage* **8**, 309–334 (2000).
- 576 38. Durinck, S., Spellman, P. T., Birney, E. & Huber, W. Mapping identifiers for the integration of  
577 genomic datasets with the R/ Bioconductor package biomaRt. *Nat. Protoc.* **4**, 1184–1191 (2009).
- 578 39. Lories, R. J., Corr, M. & Lane, N. E. To Wnt or not to Wnt: the bone and joint health dilemma. *Nat.*  
579 *Rev. Rheumatol.* **9**, 328–339 (2013).
- 580 40. Rudnicki, J. A. & Brown, A. M. Inhibition of chondrogenesis by Wnt gene expression in vivo and in  
581 vitro. *Dev. Biol.* **185**, 104–118 (1997).
- 582 41. Hoffmann, A. & Gross, G. BMP signaling pathways in cartilage and bone formation. *Crit. Rev.*  
583 *Eukaryot. Gene Expr.* **11**, 23–45 (2001).
- 584 42. Salazar, V. S., Gamer, L. W. & Rosen, V. BMP signalling in skeletal development, disease and  
585 repair. *Nat. Rev. Endocrinol.* **12**, 203–221 (2016).
- 586 43. Akkiraju, H. & Nohe, A. Role of Chondrocytes in Cartilage Formation, Progression of Osteoarthritis  
587 and Cartilage Regeneration. *J Dev Biol* **3**, 177–192 (2015).
- 588 44. GeneCards Human Gene Database. PRG4 Gene - GeneCards. [https://www.genecards.org/cgi-](https://www.genecards.org/cgi-bin/carddisp.pl?gene=PRG4&keywords=PRG4)  
589 [bin/carddisp.pl?gene=PRG4&keywords=PRG4](https://www.genecards.org/cgi-bin/carddisp.pl?gene=PRG4&keywords=PRG4).
- 590 45. Kwon, H. *et al.* Surgical and tissue engineering strategies for articular cartilage and meniscus repair.  
591 *Nat. Rev. Rheumatol.* **15**, 550–570 (2019).
- 592 46. Zhang, L., Hu, J. & Athanasiou, K. A. The role of tissue engineering in articular cartilage repair and  
593 regeneration. *Crit. Rev. Biomed. Eng.* **37**, 1–57 (2009).
- 594 47. Sophia Fox, A. J., Bedi, A. & Rodeo, S. A. The basic science of articular cartilage: structure,  
595 composition, and function. *Sports Health* **1**, 461–468 (2009).
- 596 48. Usami, Y., Gunawardena, A. T., Iwamoto, M. & Enomoto-Iwamoto, M. Wnt signaling in cartilage

- 597 development and diseases: lessons from animal studies. *Lab. Invest.* **96**, 186–196 (2016).
- 598 49. Monteagudo, S. & Lories, R. J. Cushioning the cartilage: a canonical Wnt restricting matter. *Nat.*  
599 *Rev. Rheumatol.* **13**, 670–681 (2017).
- 600 50. Wang, W., Rigueur, D. & Lyons, K. M. TGF $\beta$  signaling in cartilage development and maintenance.  
601 *Birth Defects Res. C Embryo Today* **102**, 37–51 (2014).
- 602 51. Rodríguez Ruiz, A. *et al.* Cartilage from human-induced pluripotent stem cells: comparison with  
603 neo-cartilage from chondrocytes and bone marrow mesenchymal stromal cells. *Cell Tissue Res.*  
604 (2021) doi:10.1007/s00441-021-03498-5. Online ahead of print.
- 605 52. Love, M. I., Huber, W. & Anders, S. Moderated estimation of fold change and dispersion for RNA-  
606 seq data with DESeq2. *Genome Biol.* **15**, 550 (2014).
- 607 53. Alexa, A. & Rahnenfuhrer, J. *topGO: Enrichment Analysis for Gene Ontology*. (2021).
- 608 54. Yu, G., Wang, L.-G., Han, Y. & He, Q.-Y. clusterProfiler: an R Package for Comparing Biological  
609 Themes Among Gene Clusters. *OMICS* **16**, 284–287 (2012).
- 610 55. Szklarczyk, D. *et al.* STRING v11: protein–protein association networks with increased coverage,  
611 supporting functional discovery in genome-wide experimental datasets. *Nucleic Acids Res.* **47**, 607–  
612 613 (2019).

613

## 614 **Acknowledgements**

---

615 The authors would like to acknowledge the University of Minnesota Masonic Cancer Center Comparative  
616 Pathology Shared Resource for excellent technical support by [Paula Overn](#) in the performance of all  
617 histology sample preparation and performance of immunohistochemical staining, and Dr. Katalin Kovacs  
618 for performing the histomorphometric analysis of the MTOs. The University of Minnesota Genomics  
619 Center kindly assisted by generating the Illumina sequencing data reported herein. The authors  
620 acknowledge the Minnesota Supercomputing Institute (MSI) at the University of Minnesota for providing

621 resources that contributed to the research results reported within this paper. Figures were created or  
622 organized using BioRender (biorender.com).

623 Research reported in this publication was supported by the National Center for Advancing Translational  
624 Sciences of the National Institutes of Health Award Numbers grant UL1TR002494 and UL1TR002377.  
625 The content is solely the responsibility of the authors and does not necessarily represent the official views  
626 of the National Institutes of Health. Additional support was provided from the Minnesota Partnership for  
627 Biotechnology and Medical Genomics through the Translational Product Development Fund (TPDF).  
628 The study was also supported by internal University of Minnesota grants from the Faculty Research  
629 Development Grants fund, the College of Veterinary Medicine Comparative Medicine Signature Grant  
630 Program, and the Institute for Engineering in Medicine collaborative grants program.

## 631 **Ethics declarations**

---

### 632 **Competing interests**

633 Timothy D. O'Brien, Beth Lindborg, Amanda Vegoe are officers of, and hold equity in, Ferenc Toth is a  
634 consultant for, and Yi Wen Chai is an employee of, Sarcio Inc., which has an option from the University  
635 of Minnesota to commercialize the organoid technology described herein. These interests have been  
636 reviewed and managed by the University of Minnesota in accordance with its Conflict of Interest policies.  
637 Manci Li and Peter A. Larsen declare no competing interests.

## 638 **Supplementary Information**

---

639 Supplementary Information: Supplementary information

640 Supplementary Table 1: TableS1\_15vs8\_DGE.csv

641 Supplementary Table 2: TableS2\_MarkerGenes.csv

642 Supplementary Table 3: TableS3\_decreased\_enrichment.tsv

- 643 Supplementary Table 4: TableS4\_increase\_enrichment.tsv
- 644 Supplementary Table 5: TableS5\_enrichment.NetworkNeighborAL\_decreased.tsv
- 645 Supplementary Table 6: TableS6\_enrichment.NetworkNeighborAL\_increased.tsv
- 646 Supplementary Table 7: TableS7\_ExpressionTable\_for\_Table2.xlsx
- 647 Supplementary Table 8: TableS8\_ExpressionofChondrocyteSpecificGenes.csv
- 648 Supplementary Table 9: TableS9\_Pearson\_Correlaiton\_Table.csv

649

650 **Tables**

651 **Table 1. Top local network clusters (STRING)**

<b>term ID</b>	<b>term description</b>	<b>observed gene count</b>	<b>background gene count</b>	<b>strength</b>	<b>false discovery rate</b>
<b>Decreased</b>					
CL:5705	frizzled binding, and Wnt-protein binding	5	41	1.75	7.61E-06
CL:5698	Wnt signaling pathway, and TGF-beta signaling pathway	7	186	1.24	9.06E-06
CL:5709	Wnt, and Wnt-protein binding	4	30	1.79	2.25E-05

CL:5710	Negative regulation of TCF-dependent signaling by WNT ligand antagonists, and Frizzled/Smoothed, transmembrane domain	3	18	1.89	0.0002
<b>Increased</b>					
CL:5923	TGF-beta signaling pathway, and DAN domain	12	74	1.58	4.61E-13
CL:5698	Wnt signaling pathway, and TGF-beta signaling pathway	15	186	1.28	5.03E-13
CL:5925	TGF-beta signaling pathway, and Regulation of signaling by NODAL	11	64	1.61	1.04E-12
CL:5929	Signaling by BMP, and BMP receptor binding	6	19	1.87	3.08E-08

652

653 **Table 2. Change of gene expression in biological processes (GO) of interest**

<b>GO Terms</b>	<b>Description</b>	<b>Count in network<sup>1</sup></b>	<b>p-value<sup>2</sup></b>	<b>Significance of increase<sup>3</sup></b>
<b>GO:0061036</b>	<b>positive regulation of cartilage development</b>	<b>29/32</b>	<b>0.0053</b>	<b>**</b>
<b>GO:0060591</b>	<b>chondroblast differentiation</b>	<b>4/5</b>	<b>0.0039</b>	<b>**</b>
<b>GO:0060536</b>	<b>cartilage morphogenesis</b>	<b>8/11</b>	<b>0.019</b>	<b>*</b>

GO:0003417	growth plate cartilage development	18/18	0.058	
GO:0061037	negative regulation of cartilage development	26/32	0.17	
GO:0032331	negative regulation of chondrocyte differentiation	21/25	0.17	
GO:0003413	chondrocyte differentiation involved in endochondral bone morphogenesis	15/15	0.24	
<b>GO:0061975</b>	<b>articular cartilage development</b>	<b>3/3</b>	<b>0.031</b>	*
GO:0060532	bronchus cartilage development	2/2	0.8	
GO:0060534	trachea cartilage development	6/9	0.6	

654 <sup>1</sup> number of genes expressed/genes associated with the GO term (retrieved by biomaRt v2.46.3)

655 <sup>2</sup> one-tailed Wilcoxon test comparing normalized and log-transformed transcript counts between week 8  
656 and week 15

657 <sup>3</sup> \*, p-value<0.05; \*\*, p-value <0.01

658

659

660